Weierstraß-Institut
für Angewandte Analysis und Stochastik

im Forschungsverbund Berlin e.V.

Preprint ISSN 0946 – 8633

Control of Rayleigh-Bénard Convection

Barbara Wagner[1], Andrea L. Bertozzi[2], Laurens E. Howle[3]

submitted: November 1, 2002

[1] Weierstrass Institute for Applied Analysis and Stochastics
Mohrenstrasse 39
D – 10117 Berlin
Germany
E-Mail: wagnerb@wias-berlin.de

[2] Depts. of Mathematics and Physics, Duke University, USA

[3] Dept. of Mech. Engineering and Material Science, Duke University, USA

No. 780
Berlin 2002

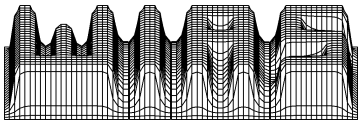

1991 *Mathematics Subject Classification.* 76R05, 76E06, 76E15, 37L65, 93A30.

Key words and phrases. Hydrodynamic stability, Galerkin method, Mathematical modeling.

Edited by
Weierstraß-Institut für Angewandte Analysis und Stochastik (WIAS)
Mohrenstraße 39
D — 10117 Berlin
Germany

Fax: + 49 30 2044975
E-Mail: preprint@wias-berlin.de
World Wide Web: http://www.wias-berlin.de/

Abstract

We consider the problem of active feedback control of Rayleigh-Bénard convection via shadowgraphic measurement. Our theoretical studies show, that when the feedback control is positive, i.e. is tuned to advance the onset of convection, there is a critical threshold beyond which the system becomes linearly ill-posed so that short-scale disturbances are greatly amplified. Experimental observation suggests that finite size effects become important and we develop a theory to explain these contributions.

As an efficient modelling tool for studying the dynamics of such a controlled pattern forming system, we use a Galerkin approximation to derive a dimension reduced model.

1 Introduction

Few problems have received as much attention from scientists and mathematicians studying nonlinear pattern-forming phenomena as the canonical Rayleigh-Bénard problem ([1, 2, 18]). In this problem, a horizontal fluid layer is heated uniformly on the underside and cooled uniformly on the upper side. The primary interest in the behavior of the Rayleigh-Bénard problem stems from the rich variety of bifurcations and chaotic dynamics that are possible ([5, 7]. Part of the appeal of the Rayleigh-Bénard system is the relative ease with which precision laboratory experiments may be conducted. This provides easy comparison of theoretical predictions with quality data. Since the pioneering work of Busse ([3, 4]) on wave pattern selection, the Rayleigh-Bénard system has evolved into an area of research in its own right.

Recent interest in controlling or suppressing fluid flow is motivated by practical applications such as Czochralski crystal growth ([15]) which is used to manufacture silicon wafers for the electronics industry. During the Czochralski crystal growth process, convection in the melt causes inhomogeneity of dopant that limit performance of integrated circuits made from the silicon wafers. Thus, the general problem of how one controls body force driven convection is an area of practical as well as scientific interest. In this paper, we consider the problem controlling convection in the Rayleigh-Bénard system.

The first work, by [19] on actively controlled convection in the Rayleigh-Bénard system, considered control through perturbation of the lower boundary temperature in proportion to the temperature at the mid-height of the fluid layer. In this configuration, the mid-height temperature profile departs from a known constant value only when convective currents are present in the layer. Using the pattern created by the flow, the convective currents can be canceled by imposing a temperature profile or heating rate profile on the lower boundary. The controller effectively boosts the natural dissipative mechanisms of heat diffusion and molecular diffusion. [19] also considered control actuation by generating a velocity profile at the lower boundary. Near the onset of convection in the Rayleigh-Bénard problem, the flow velocities are small when

compared to another characteristic velocity - the thermal diffusion velocity, τ/d where τ is the thermal diffusivity and d is the length scale of the problem - in this case the layer height. As a result, small velocities are sufficient to move the eigenvalues of the linearized perturbation system. Due to the ease of experimental realization, the thermal control method that [20] suggested is a more interesting actuation method. Also applicable to the present work is the [21] study of convection control with Joule heating at the lower boundary. Imposing a given flux at a boundary is far easier that imposing a given temperature. In the work considered in this paper, we use Joule heating at the lower boundary since this matches our experimental investigations ([9, 10, 13]).

The active control method used in Howle's experiments requires measurement of the state of the system. In the experiments, he used shadowgraphic visualization to measure the wave pattern. A controller then used this wave pattern information as an input to the control law. In order to include the wave pattern measurement in the linear analysis [11] used the expression for shadowgraphic wave pattern derived by [16]. By including the measurement and actuation in the stability analysis he could study the influence of the controller on the stability of convection.

In the work of [11], Howle studied the linear stability of a horizontally infinite fluid layer subject to control actuation. He chose no-slip flow boundary conditions at the upper and lower boundaries and an isothermal upper temperature boundary condition. The lower boundary condition used a control law simulating his experiments. The control law specifies the spatial distribution of the lower boundary heat flux while holding the spatial mean heat flux constant. This allows the controller to place heating so as to aid the natural dissipation in the system.

In [11] he could show that negative feedback control delays the onset of convection in a horizontally unbounded fluid layer. he also found that the delay in the onset of convection remains bounded for $g \to \infty$, where g denotes the negative feedback control parameter. In this limit the reduced Rayleigh number approaches the value $Ra_\infty/Ra_0 \to 3.180$, see also [17], where even higher values of Ra_∞/Ra_0 could be determined. Furthermore, Howle found that the wavenumber is bounded for negative feedback control.

Although the emphasis of experimental and theoretical studies has so far been on the delay of the onset of the instability, for many applications it is desirable to advance the onset, for example to enhance mixing in biological and chemical reactions. The focus of this study is the response of a pattern forming system, here Rayleigh-Bénard convection, to positive feedback control.

We find, that unless we include details of the controlling boundary, such as thickness of the boundary or size of the heaters, the controlled Rayleigh-Bénard problem is linearly ill-posed for sufficiently strong positive control. This property has no counterpart in the regime of negative feedback control when the onset is being delayed. The ill-posedness is removed by additional cutoff length scales in the system provided by either thin diffusive boundaries and a finite heater size which is small compared to the dominant wavelength of the instability for the uncontrolled system.

The models for our experiments that take all these effects into account show a considerable amount of complexity. This means that in order to understand the stability behavior of the system we need to make several numerical and asymptotic parameter studies. For this purpose

we find it useful to use reduced dimension models that enable us to efficiently determine and understand the key properties of the system.

The primary instability in Rayleigh-Bénard convection, as well as in many other pattern forming systems such as the fingering instability in thin film flows, have fine scale structures in some of the space dimensions with larger scale coherent in the other dimension, here the vertical direction. The idea of the Galerkin approximation method is to represent the flow variables by a linear combination of basis function, using only a small number of low degree polynomials for the vertical direction. As a consequence of the resulting reduction in dimension, analytical as well as numerical treatment of the nonlinear problem simplify and computation times are cut significantly. The idea for such an approximation has been suggested by Manneville ([14] ch. 4. sec. 2.4) for Rayleigh-Bénard with homogeneous boundary conditions, and analytical study of this problem by [6]. We extend this approach for our problem with control boundaries. Here, we need to be able to resolve also the small horizontal length scale introduced by the heaters without increasing the resolution in the vertical direction. A more detailed treatment of the mathematical theory, together with convergence results of the Galerkin approximation, is given in a companion paper [22].

In section 2, we introduce the experimental apparatus, which includes the convection layer and the network of heaters on the lower boundary. We then describe the shadowgraphic visualization procedure used to gather data and finally the control activation. In section 3, we introduce the governing equations for the basic controlled system, and explain how the control boundary condition arises naturally for the experimental setup. In section 4, we discuss why and where this model becomes ill-posed through a linear stability analysis which shows a blow up of the growth rate for short wave perturbations. In section 5, we model the effects of finite heater size and finite boundary thickness. For the resulting system we derive and investigate, in section 6, a dimension reduced model based on a Galerkin approximation.

2 Experimental Method

2.1 Convection Layer

In figure 1, we show a drawing of the convection layer used in these experiments. The $d = 0.794cm$ high fluid layer has horizontal aspect ratios of $\Gamma = 1.6, 8.0$. The fluid layer uses glass microscope slides as the lower and upper boundaries. The lower boundary is coated with a 300 layer of Cr on the upper side (side toward the fluid). This produces a reflective surface for use with shadowgraphic visualization. On the lower side of the lower boundary, a 1200 layer of Au is deposited upon a 300 layer of Cr. We then etch the heater network shown in figure 2. The width of each $252 \pm 2\Omega$ heater wire is $100\mu m$. This heater array provides twenty individually controlled heaters each of which is capable of depositing $8W$ of heating (orders of magnitude more than needed) into the glass substrate. Under normal operating conditions, the 100 hour resistance change of the heaters is $< 0.1\%$.

An uncoated microscope slide serves as the upper boundary. A Neslab RTE-221 computer controlled bath circulator holds the temperature of the upper boundary constant.

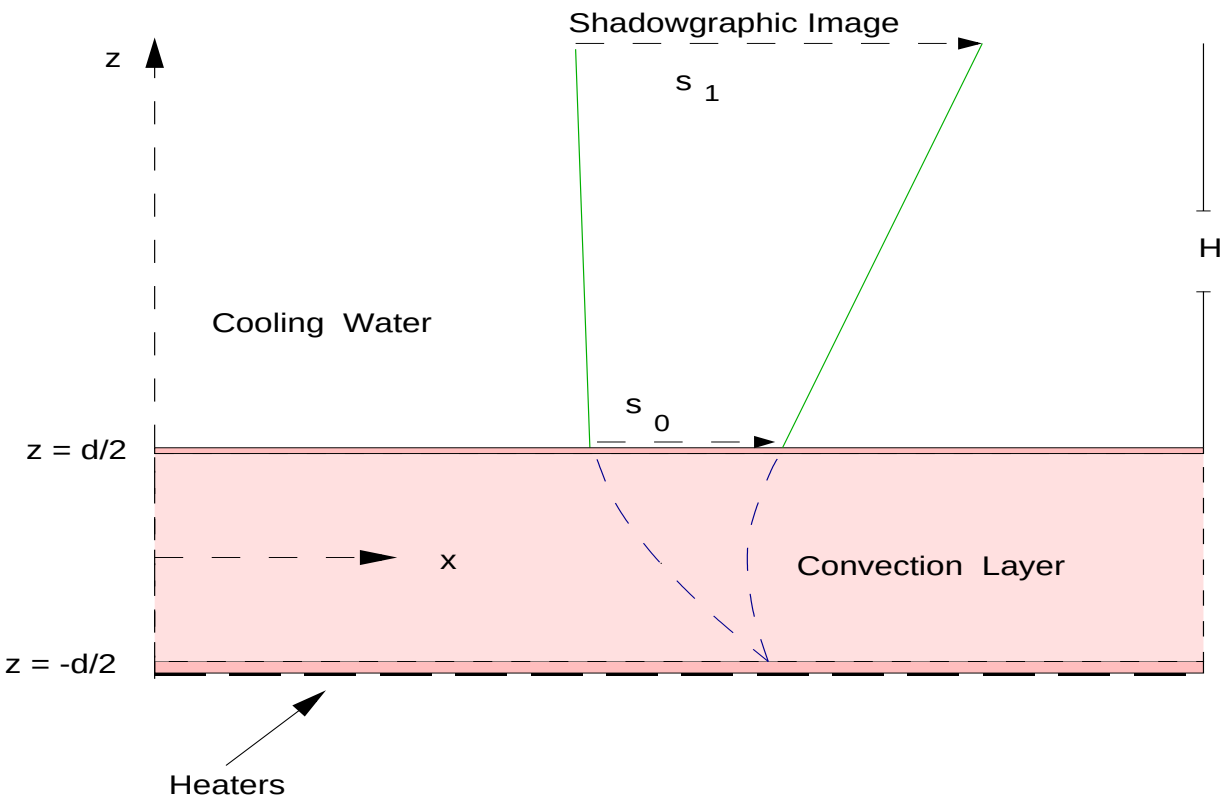

Figure 1: Drawing of the convection control apparatus

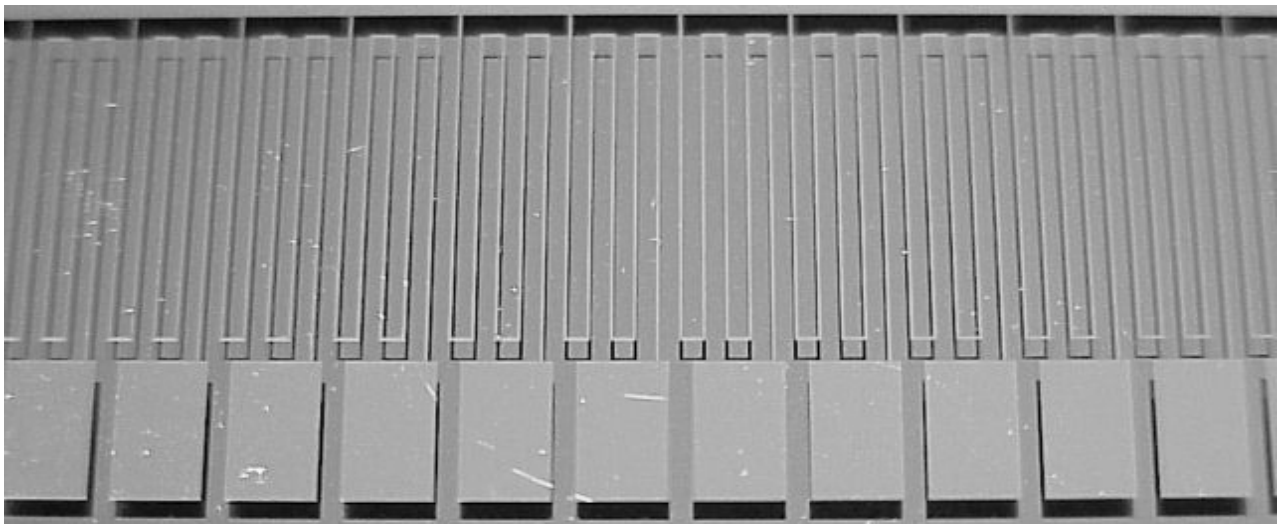

Figure 2: Heater pattern etched into the convection layer lower boundary.

2.2 Visualization System

Wave pattern information for convection amplitude measurement and for feedback control input is measured by a shadowgraph (see Figure 1). Consider in figure 1 a laser beam that enters the fluid layer vertically. The reflected beam will also leave the layer vertically, unless there is a horizontal gradient in the depth averaged temperature. In the latter case the reflected beam is tilted at an angle proportional to the local gradient. For a constant temperature gradient everywhere in the fluid layer, the tilt angle is constant for all x-positions. Consequently we would obtain a shadowgraphic image of uniform brightness, virtually identical to the situation without any gradient in the depth averaged temperature. Only when the tilt angle varies spatially does the CCD camera record nonuniformities in the brightness of the shadowgraphic images which are used to adjust the heat flux at the lower boundary using linear proportional gain. Therefore only deviations of the temperature gradient enter the control boundary condition (3.16).

As a measure of convection amplitude, we use the standard deviation of the shadowgraph. We choose this rather than the more commonly used Nusselt number for experimental convenience. In order to measure the Nusselt number, we would need to take many point temperature measurements along the lower boundary. This would not only be difficult but would also introduce additional thermal capacitance at the lower boundary as thermistors are not negligibly small compared to the apparatus. In a steady-state experiment this would not present a problem. In a control experiment, however, the temperature of the lower boundary must be continually perturbed. Additional capacitance introduced by thermistors will lower the gain at which the primary bifurcation changes from stationary convection to time-dependent convection ([11]).

2.3 Control Activation

The convection image read by camera-frame grabber is digitized by the P5 computer. The computer bins the image into twenty regions, each corresponding to a heater. Since the image has a nonuniform intensity caused by the Gaussian intensity distribution of the laser, we normalize each bin by subtracting the pre-convection intensity and then dividing the difference by the pre-convection intensity. The control law is then applied to a weighted sum of local intensities using the weight function

$$I_i' \;=\; \frac{I_{i-1} \;+\; 2I_i \;+\; I_{i+1}}{4} \tag{2.1}$$

with the end heaters using a non-centered weight function. For example, the weight function for the first heater is

$$I_1' \;=\; \frac{2I_i \;+\; I_{i+1} \;+\; I_{i+2}}{4} \quad . \tag{2.2}$$

Our choice of these weight functions is arbitrary and seems to produce slightly better results than a unit weight function at region i.

For the results given in this paper, we use a linear proportional control law. We have also used linear proportional-differential control, nonlinear control, are presently using fuzzy logic control, but will focus in this paper on linear control. Our control law is

$$q_i \;=\; \bar{q}\,(1 \;+\; gI_i')\;, \tag{2.3}$$

where g is the proportional gain, q_i is the heat flux supplied to region i, and $\bar{q}$ is the mean heat flux. This is the same control law we studied by linear stability analysis for controlled Rayleigh-Bénard convection ([10]), for controlled Rayleigh-Bénard convection with horizontal boundaries ([11]), for controlled convection in porous media with horizontal boundaries ([8]).

Once the shadowgraph is acquired and processed and the control law (2.3) applied, the heaters are set to the power q_i by a power amplifier system.

3 Mathematical Formulation

The governing equations for the convection layer are the Boussinesq approximation together with continuity and energy equation. In dimensionless form,

$$T^+ = T + \theta_u - (z - \frac{1}{2}), \tag{3.4}$$

$$p^+ = p + R(\theta_u + 1/2)z - Rz^2/2 \tag{3.5}$$

denote the temperature and the pressure, both written as the sum of the convective and the conductive part, where θ_u is the temperature on the upper boundary. Since the conductive contribution to the velocity is zero we denote the velocity by $\boldsymbol{u} = (v, w)$. We obtain for the governing equations

$$Pr^{-1}\left[\partial_t \boldsymbol{u} + (\boldsymbol{u} \cdot \boldsymbol{\nabla})\,\boldsymbol{u}\right] = -\boldsymbol{\nabla} p^+ + R\; T^+\; (0,1)^t + \nabla^2 \boldsymbol{u}\,, \tag{3.6}$$

$$\boldsymbol{\nabla} \cdot \boldsymbol{u} = 0\,, \tag{3.7}$$

$$\partial_t T + \boldsymbol{u} \cdot \boldsymbol{\nabla} T = \nabla^2 T + w\,, \tag{3.8}$$

where the scalings

$$\left.\begin{array}{rclrclrcl} (x,z) &=& (\dfrac{x^*}{d}, \dfrac{z^*}{d}), & t &=& \dfrac{\kappa}{d^2} t^*, & (v,w) &=& \dfrac{d}{\kappa}(v^*, w^*), \\ T^+ &=& \dfrac{k}{\bar{q} d} T^*, & p &=& \dfrac{d^2}{\rho \kappa^2} p^*, & & & \end{array}\right\} \tag{3.9}$$

have been used. We denote by d, κ, ρ and $\bar{q}$ the height of the fluid layer, thermal diffusivity, fluid density and spatially averaged heat flux, respectively.

$$R = \frac{g\alpha \bar{q} d^4}{\kappa \nu k_{th}} \quad \text{and} \quad Pr = \frac{\nu}{\kappa} \tag{3.10}$$

denote the Rayleigh and the Prandtl number, with k_{th}, α, g and ν the thermal conductivity, thermal expansion coefficient, gravity and viscosity, respectively. In our experiments $Pr \sim 200$ and we therefore neglect the left hand side of (3.6) in our subsequent analysis.

For the boundary conditions we assume no-slip and impermeability for the velocity at the upper and lower boundaries

$$v = w = 0 \qquad \text{at} \quad z = \pm\frac{1}{2}\,. \tag{3.11}$$

Since the temperature is kept fixed at the upper boundary we have

$$T = 0 \qquad \text{at} \quad z = +\frac{1}{2}\,. \tag{3.12}$$

In order to control the heat flux

$$q = -k_{th}\ \partial_{z^*} T^* \tag{3.13}$$

at the lower boundary we set q proportional to the shadowgraphic signal. In the article by [16] an expression for the intensity distribution of the shadowgraphic field in terms of the average temperature $\int_{-d/2}^{d/2} T^* dz^*$, under the condition that

$$\frac{d}{H} \ll 1 \quad \text{and} \quad \frac{|s_0|}{|s_1|} \ll 1\,,$$

(see figure 1), could be derived as

$$\frac{\delta I(x^*)}{I_0} = -2H \frac{d\eta}{dT^*} \partial_{x^*}^2 \int_{-d/2}^{d/2} T^* dz^*\,. \tag{3.15}$$

Upon substitution of the expression for $q = \bar{q}(1 + g\delta I(x^*)/I_0)$ into (3.13) we obtain for the remaining boundary condition

$$\partial_z T = -\varepsilon\ \partial_x^2 \int_{-1/2}^{1/2} T\, dz \qquad \text{at} \quad z = -\frac{1}{2}, \tag{3.16}$$

where

$$\varepsilon = \frac{2gH}{d}\left(-\frac{d\eta}{dT}\right)$$

is the control parameter. Note that for most fluids the refractive index η decreases with temperature. Note, also, that the mean heat flux per unit length is not altered by the control, since

$$\frac{1}{L}\int_0^L \left(\partial_x^2 \int_{-1/2}^{1/2} T\, dz\right)\, dx = 0 \tag{3.18}$$

if we impose for example homogeneous Neumann boundary conditions at the side walls of the container. This remains also true in the limit $L \to \infty$, i.e. for sufficiently long (in x-direction) containers, with bounded heat flux at the side walls. Naturally, equation 3.18 is satisfied for any periodic temperature distribution. As a consequence, the global Rayleigh number remains unchanged.

4 Ill-posedness for positive feedback

The above formulation adds the control boundary condition (3.16) to the standard model for Rayleigh-Bénard convection . This control mechanism is quite effective. Linear stability

analysis of the model ([11]) predicts a significant increase in the critical Rayleigh number for positive ε. This delay of the onset of the instability agrees well with experimental results.

In this paper we concentrate on the case of using the controller to introduce positive feedback. For negative ε, the convective instability is enhanced. Moreover beyond a critical value of the control parameter, the model becomes ill-posed; short wave disturbances experience arbitrarily large growth rates. This is a direct consequence of the presence of the second derivatives in (3.16).

4.1 Ill-posedness of the heat equation with positive control

First consider the heat equation alone,

$$\partial_t T = \nabla^2 T, \tag{4.19}$$

coupled to the control boundary condition (3.16). This is a linear equation and we can easily determine its well-posedness for different values of the control ε using separation of variables methods.

As a preliminary calculation, we consider first, instead of the constant boundary condition (3.12), the no-flux temperature condition on the top boundary,

$$T_z = 0 \quad \text{at} \quad z = \frac{1}{2}. \tag{4.20}$$

Integrating (4.19) from $z = -1/2$ to $z = 1/2$ and taking the Fourier transform in x gives

$$\partial \tilde{T}(k) = -(\varepsilon + 1)k^2 \tilde{T}(k), \quad \tilde{T} = \int_{-1/2}^{1/2} \int e^{-ikx} T(x, z) dx dz. \tag{4.21}$$

We see that the resulting one-dimensional spectrum decays like a diffusion process with coefficient $-(\varepsilon + 1)$ provided $\varepsilon > -1$. For $\varepsilon < -1$ we obtain a backward-time diffusion process and the the problem is ill-posed: perturbations at high wave number k are amplified at rate that scales as k^2 and classical solutions to the forward-time problem do not exist.

We now show that this same ill-posedness results when the no-flux boundary condition (4.20) is replaced with a constant temperature condition (3.12). The above trick no longer works so we solve the full problem using separation of variables. To first simplify, we Fourier transform (4.19) in x to obtain a one-dimension heat equation in the variable z:

$$\hat{T}_t = \hat{T}_{zz} - k^2 \hat{T}, \tag{4.22}$$

with boundary conditions (3.12) and (3.16). We look for a solution of the form $\hat{T}(z, t; k) = f(z; k)e^{\sigma(k)t}$. Plugging this into (4.22) gives a transcendental equation for σ,

$$\frac{\varepsilon k^2}{\sigma + k^2(\varepsilon + 1)} = \begin{cases} \cosh(\sqrt{k^2 + \sigma}), & k^2 + \sigma \geq 0 \\ \cos(\sqrt{k^2 + \sigma}), & k^2 + \sigma < 0. \end{cases} \tag{4.23}$$

With the change of variables $\alpha = 1 + \sigma/k^2$, (4.23) simplifies to

$$\frac{\varepsilon}{\alpha + \varepsilon} = \begin{cases} \cosh(k\sqrt{\alpha}), & \alpha \geq 0 \\ \cos(k\sqrt{\alpha}), & \alpha < 0. \end{cases} \tag{4.24}$$

We are interested in when (4.24) has roots $\alpha > 1$, which imply instability and possible ill-posedness. First we consider the case $\varepsilon > 0$. For this case one can check that the largest root is $\alpha = 0$ which corresponds to the null eigenfunction and thus must be discarded. Smaller roots α_n exist are increasingly more negative, scaling like $-(2n+1)^2\pi^2/4k^2$ $n \to \infty$.

In the case $-1 \leq \varepsilon < 0$, the roots are all less than one, indicating stability. However there is a single root α_0 that lies between zero and one when k is sufficiently large, $k > -2/\varepsilon$. For large k, $\alpha \sim -\varepsilon$ which means $\sigma \sim (-\varepsilon - 1)k^2$, i.e. for large k the largest eigenvalue aligns with the largest eigenvalue for the problem with a no-flux boundary condition (4.20).

For $\varepsilon < -1$ there is a positive root whenever $k > -2/\varepsilon$. That root also yields $\sigma \sim (-\varepsilon - 1)k^2$ for large k, as in the no-flux case. In particular, the problem with constant temperature boundary condition (3.12) is ill-posed for $\varepsilon < -1$. Furthermore, we find that for complex eigenvalues σ the real and imaginary parts of the corresponding transcendental equation have no solution for $\varepsilon < 0$, while all solutions that do exist for $\varepsilon > 0$ decay.

4.2 Ill-posedness for the full Rayleigh-Bénard system with positive control

We now consider the full system and linearize (3.6)–(3.8), (3.11)–(3.12) and (3.16) about their conductive state and using the normal mode ansatz

$$T(x,z,t) = \Theta(z)e^{\sigma t + ikx}\,,$$

$$w(x,z,t) = W(z)e^{\sigma t + ikx}\,,$$

with growth rate σ and wavenumber k we obtain the following linear eigenvalue problem for the amplitude of the temperature $\Theta(z)$ (see [11]) :

$$(\partial_z^2 - k^2)^2(\partial_z^2 - k^2 - \sigma)\Theta = -k^2 R\Theta\,, \tag{4.25}$$

$$(\partial_z^2 - k^2 - \sigma)\Theta\left(\pm\frac{1}{2}\right) = 0\,, \tag{4.26}$$

$$\partial_z(\partial_z^2 - k^2 - \sigma)\Theta\left(\pm\frac{1}{2}\right) = 0\,, \tag{4.27}$$

$$\Theta\left(\frac{1}{2}\right) = 0 \quad \text{and} \quad \partial_z\Theta\left(-\frac{1}{2}\right) = \varepsilon k^2 \int_{-1/2}^{1/2} \Theta\, dz\,. \tag{4.28}$$

We then discretize these equations using a pseudo-spectral method, then solve for the leading eigenvalue by inverse vector iteration. We observe that the critical wavenumber $k_c \to \infty$ when

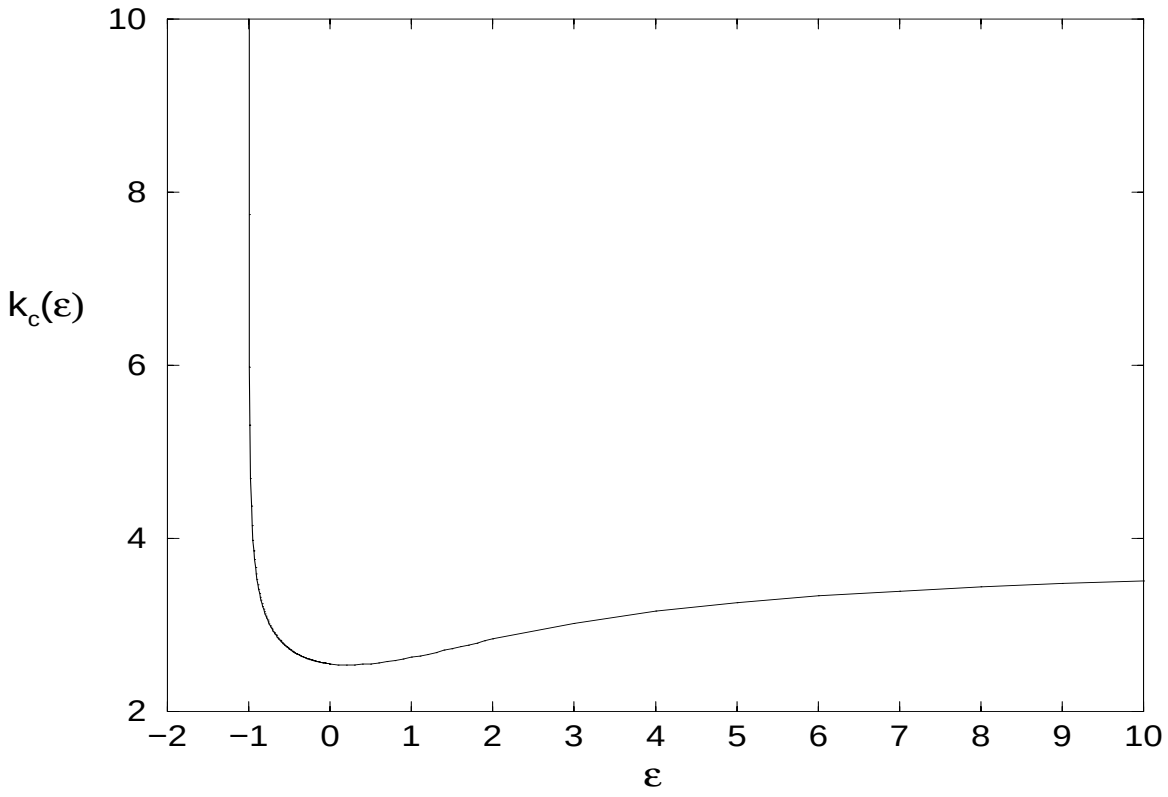

Figure 3: Critical wavenumbers $k_c(\varepsilon)$

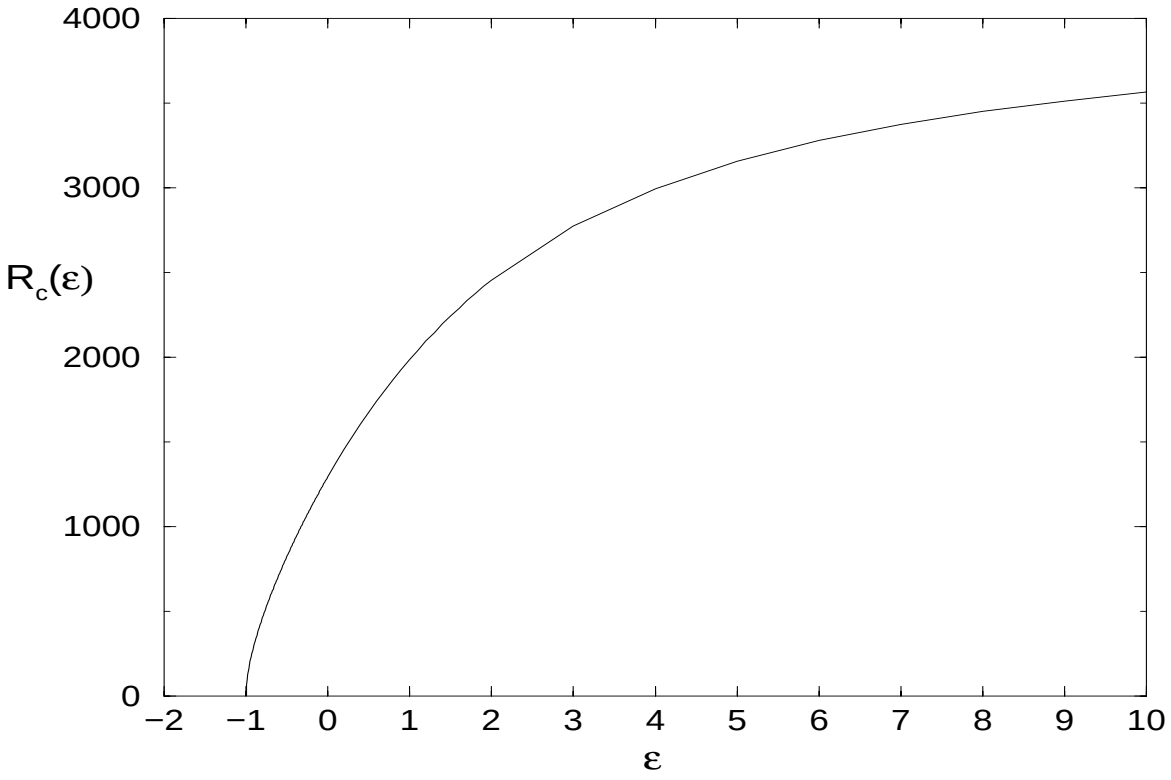

Figure 4: Critical Rayleigh numbers $R_c(\varepsilon)$

$\varepsilon \to -1$, while at the same time the critical Rayleigh number $R_c \to 0$. This can be seen in figures (3) and (4). For $\varepsilon < -1$ we find that $\sigma \to \infty$ for $k \to \infty$, i.e. the problem becomes ill-posed.

In fact, we can observe this transition straightforwardly by solving the problem (4.25)–(4.28) asymptotically for small R. To leading order the solution of (4.25)–(4.28) can be represented as

$$\begin{aligned}\Theta_0(z) &= (A_1 + A_2 z)\cosh(kz) + A_3 \cosh\left(\sqrt{k^2+\sigma}z\right) \\ &\quad +(B_1 + B_2 z)\sinh(kz) + B_3 \sinh\left(\sqrt{k^2+\sigma}z\right) \end{aligned} \tag{4.29}$$

where A_1–A_3 and B_1–B_3 are constants to be determined. If we substitute this into the boundary conditions (4.26)–(4.28), we obtain the solvability condition for the linear stability, $Det(A) = 0$, where $A = [\mathbf{v_1}, \mathbf{v_2}, \mathbf{v_3}, \mathbf{v_4}, \mathbf{v_5}, \mathbf{v_6}]$ with the column vectors

$$\begin{aligned}
\mathbf{v_1} &= \cosh(k/2)\ [-\sigma, -\sigma, -k\sigma\tanh(k/2), k\sigma\tanh(k/2), 1, -k(1+2\varepsilon)\tanh(k/2)]\ , \\
\mathbf{v_2} &= \cosh(k/2)\ \big[2k\tanh(k/2) - \sigma/2, -2k\tanh(k/2) + \sigma/2, (2k^2-\sigma) - k/2\sigma\tanh(k/2)\ , \\
&\qquad (2k^2-\sigma) - k/2\sigma\tanh(k/2), 1/2, 1 + k/2\tanh(k/2)\big]\ , \\
\mathbf{v_3} &= \left[0,0,0,0,\cosh(1/2\sqrt{k^2+\sigma}), -(\sqrt{k^2+\sigma} + 2k^2\varepsilon/(\sqrt{k^2+\sigma}))\sinh(1/2\sqrt{k^2+\sigma})\right]\ , \\
\mathbf{v_4} &= \cosh(k/2)\ [-\sigma\tanh(k/2), \sigma\tanh(k/2), -k\sigma, -k\sigma, \tanh(k/2), k]\ , \\
\mathbf{v_5} &= \cosh(k/2)\ \big[2k - \sigma/2\tanh(k/2), 2k - \sigma/2\tanh(k/2), (2k^2-\sigma)\tanh(k/2) - k/2\sigma\ , \\
&\qquad -(2k^2-\sigma)\tanh(k/2) + k/2\sigma, 1/2\tanh(k/2), -(1+\varepsilon)k + (2\varepsilon-1)\tanh(k/2)\big]\ , \\
\mathbf{v_6} &= \left[0,0,0,0,\sinh(1/2\sqrt{k^2+\sigma}), \sqrt{k^2+\sigma}\cosh(1/2\sqrt{k^2+\sigma})\right]\ .
\end{aligned}$$

For large k, the dominant contributions in $Det(A) = 0$ are

$$\cosh\left(\frac{k}{2}\right)^4 \cosh\left(\frac{\sqrt{k^2+\sigma}}{2}\right)^2 \left(\varepsilon k^2 + k^2 + \sigma\right) = 0$$

which implies

$$\sigma \sim -(1+\varepsilon)\, k^2\,, \tag{4.30}$$

the asymptotic behavior of the controlled heat equation, which is ill-posed when $\varepsilon < \varepsilon^\star = -1$.

In fact, the experiments do not directly exhibit ill-posedness, i.e. fast amplification of small wave number perturbations. As long as $\varepsilon > \varepsilon^\star$ we qualitatively have the same stability diagram for $\sigma(k)$ with a finite critical $R_c(\varepsilon)$ and $k_c(\varepsilon)$, so that for $R > R_c(\varepsilon)$ a range of wavenumbers around $k_c(\varepsilon)$ have positive growth rates. In this range of ε the instability is still buoyancy driven. For large negative ε the control itself drives the instability and the preferred wavelength approaches the limit set by the details of the control boundary such as the heater size and/or finite boundary thickness. The above model completely neglects these boundary effects. We will investigate this aspect in the following section.

5 Inclusion of boundary effects

5.1 Inclusion of finite boundary thickness

Suppose that on the boundary $z = -1/2$ there is a plate of thickness δ attached. Further, suppose the plate is thin enough so that the time-scale of heat diffusion within the plate is small compared to the time-scale of heat diffusion within the fluid layer. Hence, the temperature distribution in the plate is governed by Laplace's equation.

We consider the following problem for the temperature (3.8) with (3.16) replaced by

$$\begin{aligned} \partial_z T(x,-1/2,t) &= \theta_z(x,-1/2,t)\,, && (5.31)\\ T(x,-1/2,t) &= \theta(x,-1/2,t)\,, && (5.32)\\ \partial_x^2\theta + \partial_z^2\theta &= 0 \quad \text{for} \quad -1/2-\delta < z < -1/2\,, && (5.33)\\ \partial_z\theta(x,-1/2-\delta,t) &= -\varepsilon\,\partial_x^2 \int_{-1/2}^{1/2} T\,dz\,. && (5.34) \end{aligned}$$

If we insert the normal mode ansatz for T and accordingly for θ, then solve (5.33) together with (5.32) and (5.34) and substitute into (5.31) we obtain the new boundary condition

$$\partial_z\Theta(-1/2) = k\tanh(k\delta/2)\Theta(-1/2) + \varepsilon\frac{k^2}{\cosh(k\delta/2)}\int_{-1/2}^{1/2}\Theta\,dz\,. \qquad (5.35)$$

We now observe that for any fixed ε the second term on the right hand side of 5.35, which was responsible for the ill-posedness becomes negligible as $k \to \infty$. The first term, which only grows like $O(k)$, turns out to be innocuous.

5.2 Inclusion of finite heater size

Another effect that limits the amplification of short wave disturbances is the finite size of the heaters. Suppose, at $z = -1/2$ there are heaters distributed along the x-axes of equal, finite size λ. Let us recall how the heat flux is controlled according to the shadowgraphic signal, amplified by the proportional gain ε

$$f(x,t) = -\varepsilon\,\partial_x^2\int_{-1/2}^{1/2} T\,dz\,. \qquad (5.36)$$

Here we have assumed that the resolution of the shadowgraphic image can be neglected compared to the heater size, so that f models a continuous signal. Since we cannot control the heat flux at every continuously varying x, we uniquely assign each x-position to one of the heaters and require the j^{th} heater to emit the total heat flux of all points that have been assigned to it:

$$f_j = \int_{j\lambda}^{(j+1)\lambda} f(x,t)\,dx\,. \tag{5.37}$$

In the experiment this expression was modified by averaging f_j over neighboring heaters. We take this feature into account by setting

$$f_j = \frac{1}{\sqrt{2\pi}} \int_{-\infty}^{\infty} f(x,t)\,K(x-x_j)\,dx\,, \tag{5.38}$$

where $K(y) = \exp(-y^2/2\lambda^2)$, and $x_j = (j+1/2)\lambda$ is the center of the j^{th} heater.

If we now assume that each heater produces a Gaussian heat flux distribution, we obtain the new boundary condition

$$\partial_z T = \sum_{j=-\infty}^{\infty} f_j\,\frac{K(x-x_j)}{\sqrt{2\pi}\lambda}\,. \tag{5.39}$$

We approximate the sum in (5.39) by an in integral expression, to obtain the boundary condition

$$\begin{aligned} \partial_z T(x,-1/2,t) &= \frac{1}{2\pi\lambda^2} \int_{-\infty}^{\infty} \left(\int_{-\infty}^{\infty} f(\xi,t) K(\eta-\xi)\,d\xi \right) K(x-\eta)\,d\eta \\ &= \frac{1}{2\pi\lambda^2} (f \star K) \star K\,, \end{aligned} \tag{5.40}$$

where $\star$ denotes convolution. Note, that (5.39) is simply the trapezoidal sum for the outer convolution, so that the error we make becomes negligible for small λ.

Hence, instead of (4.28) we have

$$\partial_z \Theta(-1/2) = \varepsilon\,k^2\,e^{-k^2\lambda^2} \int_{-1/2}^{1/2} \Theta\,dz\,. \tag{5.41}$$

Clearly, from (5.41) we see that the effect of finite heater size introduces an exponentially decaying factor for $k \to \infty$, and thereby removes the ill-posedness for any given ε.

Finally, we combine the boundary effects, arising from finite boundary thickness and finite heater size to obtain a new boundary condition for the temperature at $z = -1/2$ for the linear stability problem:

$$\partial_z \Theta(-1/2) = k\tanh(k\delta/2)\Theta(-1/2) + \varepsilon\,\frac{k^2\,e^{-k^2\lambda^2}}{\cosh(k\delta/2)} \int_{-1/2}^{1/2} \Theta\,dz\,. \tag{5.42}$$

In figure 5 we compare the critical wavenumbers $k_c(\varepsilon)$ for $\delta = 0.1$ and $\lambda = 0.1$ to the situation where $\delta = 0$ and $\lambda = 0$ (dotted curve), using inverse vector iteration where applicable, i.e. as

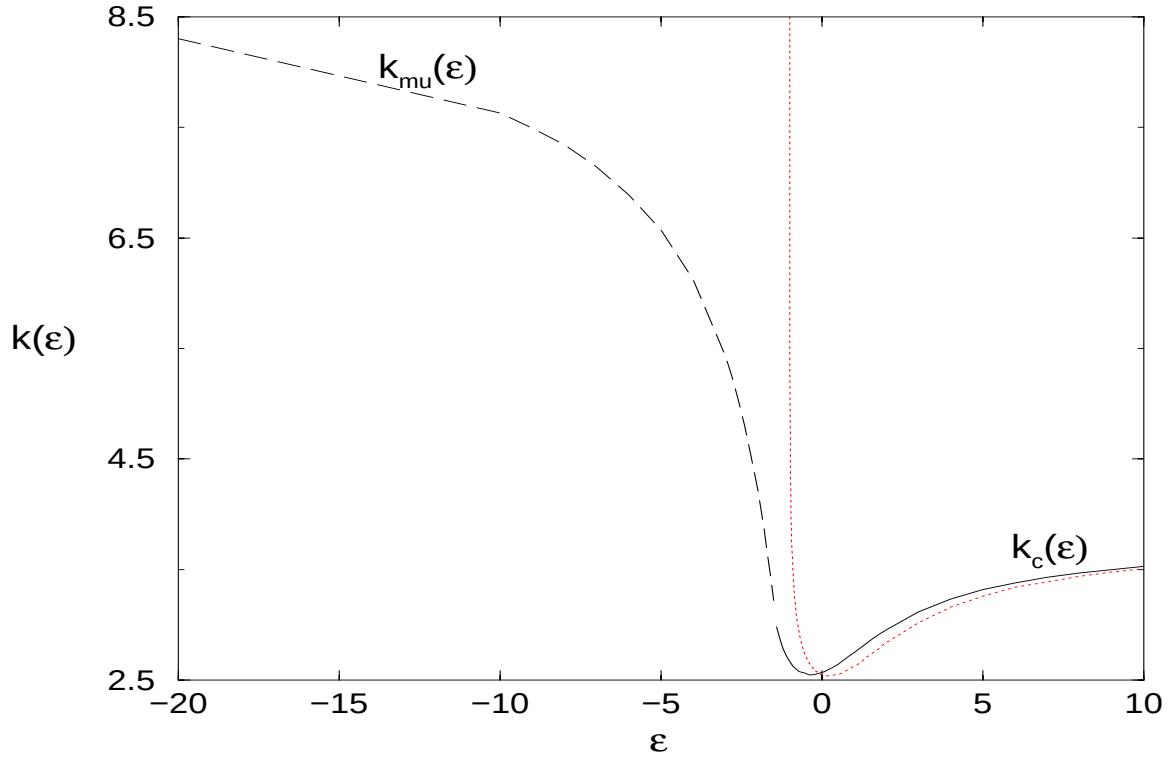

Figure 5: Critical wavenumbers $k_c(\varepsilon)$ for $\delta = 0$, $\lambda = 0$ (dotted) and $\delta = 0.1$, $\lambda = 0.1$ (solid). Most unstable wavenumbers $k_{mu}(\varepsilon)$ (dashed)

long as $R_c(\varepsilon, \delta, \lambda) > 0$. We observe that the effects of the small heater size and plate thickness are negligible (comparing solid and dotted curves) as long as ε is large. Furthermore, the critical value $\varepsilon^\star = -1$ below which the problem is ill-posed, when boundary effects are not taken into account, i.e. for $\delta = 0$, $\lambda = 0$, is now replaced by another critical value when boundary effect are accounted for, e.g. by $\varepsilon = -1.1$,for $\delta = 0.1$, $\lambda = 0.1$ (see figure 6, dashed curve), below which the problem will always be unstable with dominant wavenumber $k_{mu}(\varepsilon)$ (dashed curve).

Beyond that point, as $\varepsilon \to -\infty$ the most unstable wavenumber is eventually determined by boundary effects such as heater size and/or boundary thickness.

In the following section we will explain this and show how to determine these wavenumbers $k_{mu}(\varepsilon)$. We will also show that this can be done most conveniently by employing a reduced dimension Galerkin method.

6 Galerkin approximation method for controlled Rayleigh-Bénard convection

The idea of this approximation method is to represent the flow variables by a linear combination of basis function, using only a small number of low degree polynomials for the z-direction. By testing with the basis functions (i.e. multiplying by the basis functions and integrating over

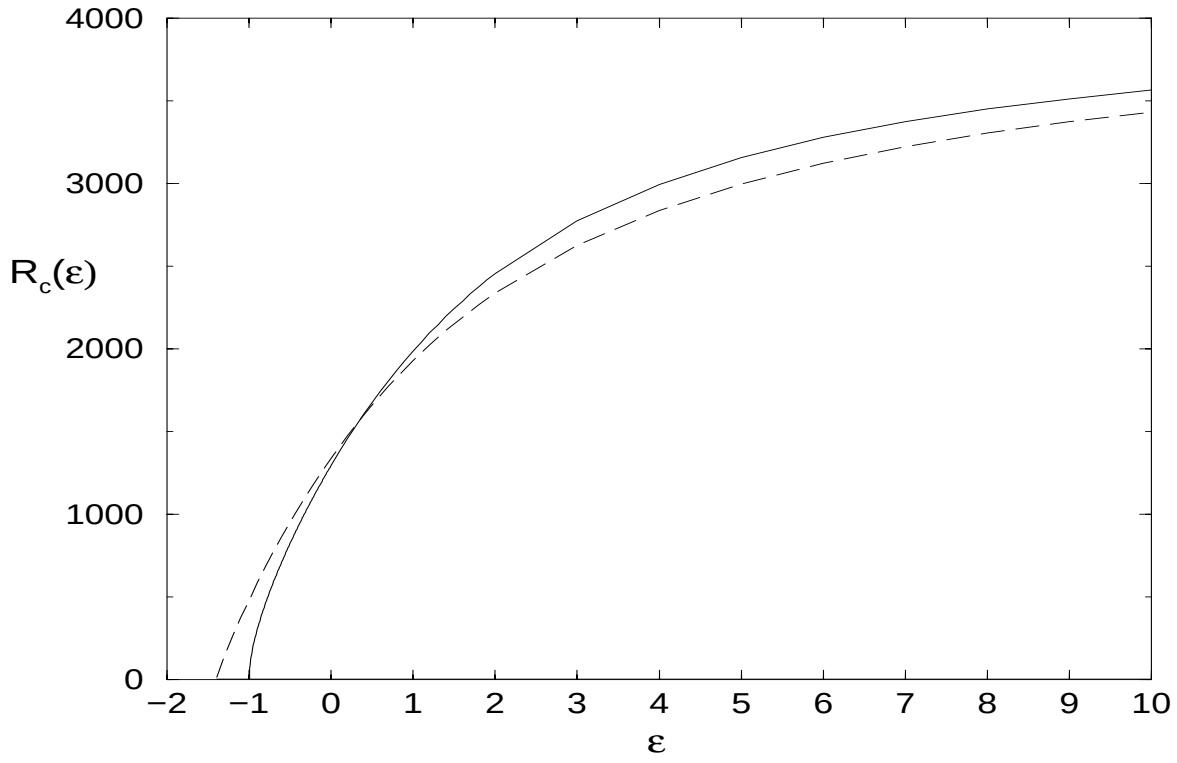

Figure 6: Critical Rayleigh numbers $R_c(\varepsilon)$ for $\delta = 0$, $\lambda = 0$ (solid) and $\delta = 0.1$, $\lambda = 0.1$ (dashed)

the domain) each equation of the governing system is replaced by a small number of lower dimension equations.

One modelling aspect of this method is to determine the minimal number of polynomials necessary to capture the dominant nonlinearity. The usefulness of this method is due to the fact that in many cases the patterns that arise in many hydrodynamic instabilities can be approximated by one or two polynomials.

6.1 Galerkin approximation

For our problem the first bifurcation state are stationary rolls. For this pattern we want to determine the minimal Galerkin basis that captures well the features of this flow.

The minimal polynomial representation for the velocity components (v, w) that satisfy the no-slip boundary and non-permeability conditions at $z = \pm 1/2$ and the continuity equation is

$$v(x, z, t) = u(x, t)\, \mu_z(z)\,, \tag{6.43}$$
$$w(x, z, t) = -u_x(x, t)\, \mu(z)\,, \tag{6.44}$$

where

$$\mu(z) = \frac{1}{4}\left(z^2 - \frac{1}{4}\right)^2\,. \tag{6.45}$$

Figure 7 shows streamlines of a roll pattern produced by (6.43)–(6.45) for periodic $u(x, t)$.

The temperature satisfies a nonhomogeneous boundary condition with feedback control. We take this into account by making the following ansatz for the Galerkin approximation of the temperature field:

$$T(x, z, t) = h(x, t)\, H_0(z) + s(x, t)\, \ell(z)\,, \tag{6.46}$$

where we have split the temperature into a contribution for the problem with homogenous boundary conditions plus a term that models the control boundary conditions.

This means that

$$H_0(1/2) = 0 \qquad \text{and} \quad H_0'(-1/2) = 0\,, \tag{6.47}$$

while

$$\ell(1/2) = 0 \qquad \text{and} \quad \ell'(-1/2) = 1\,. \tag{6.48}$$

The lowest order polynomial $H_0(z)$ that satisfies the conditions (6.47) is

$$H_0(z) = \left(z - \frac{1}{2}\right)\left(z + \frac{3}{2}\right)\,, \tag{6.49}$$

see the dashed curve in figure 8. This representation of the temperature is capable of producing temperature fields which are not symmetric with respect to zero.

Rayleigh-Bénard convection rolls diminish the temperature difference between $z = \pm 1/2$ in that they carry hot fluid from the lower side to the top (filled arrows in figure (7)), while cold

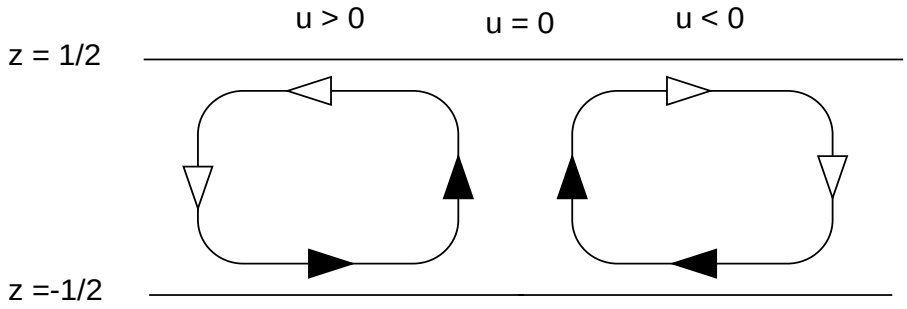

Figure 7: Streamlines for (6.43)–(6.45).

fluid will be transported from the upper side to the bottom (empty arrows). This is necessary to achieve nonlinear saturation of the rolls.

This is not so, if for example we had chosen Neumann boundary conditions on both sides, see [6]. In this case we would have needed a third order polynomial as well in order to break the symmetry of the temperature profile.

In [22] we show that the polynomial $\ell(z)$ not only needs to satisfy conditions (6.48) but in order to prevent artificial singularities that arise through this approximation, for positive feedback control, we need to require

$$\rho_1 = \int_{-1/2}^{1/2} \ell(z)\,dz = \langle \ell, H_0 \rangle \int_{-1/2}^{1/2} H_0(z)\,dz \quad \text{with} \quad \langle \ell, H_0 \rangle = \int_{-1/2}^{1/2} \ell(z) H_0(z)\,dz\,. \tag{6.50}$$

In order to simplify calculations we choose $\ell(z)$ to be orthogonal to $H_0(z)$, i.e. the scalar product $\langle \ell, H_0 \rangle = 0$, and therefore also $\rho_1 = 0$. This leads us to the following polynomial:

$$\ell(z) = \left(z - \frac{1}{2}\right)\left(z^2 + \frac{1}{8}z - \frac{1}{16}\right)\,. \tag{6.51}$$

Finally, we obtain the Galerkin approximation by testing the full problem with the test functions

$$\theta_0 = \delta(x)\,\mu_z(z)\,, \qquad \theta_1 = -\delta'(x)\,\mu_z(z)\,, \qquad \phi_0 = \delta(x) H_0(z)\,, \tag{6.52}$$

to obtain

$$\partial_x^4 u - 24\,\partial_x^2 u + 504\,u \;=\; -R\;\partial_x\left(60\,h - \frac{3}{2}\,s\right)\,, \tag{6.53}$$

$$\partial_t h - \partial_x^2 h + \frac{5}{2}h + \frac{9}{448}\left(u\partial_x h + \frac{1}{2}h\partial_x u\right) \;=\; \frac{15}{8}s + \frac{5}{448}\partial_x u + \frac{u\partial_x s - 3/2\,s\,\partial_x u}{448\cdot 24}\,, \tag{6.54}$$

$$\text{with} \quad s = \varepsilon\,\frac{2}{3}\,\partial_x^2 h \tag{6.55}$$

representing the control boundary condition.

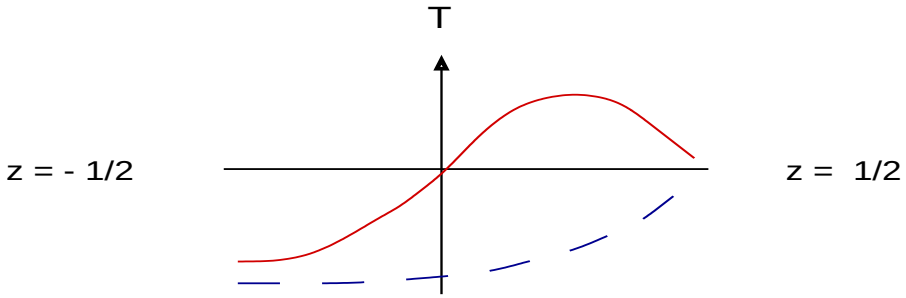

Figure 8: Polynomials for the temperature $H_0(z)$ (dashed) and $H_1(z)$ (solid)

We first observe, that for this Galerkin approximation, linearization about the conductive state $h(x,t) = 0$, $u(x,t) = 0$, reduces the linear stability problem to solving

$$\partial_t \hat{h} = \sigma(k,\varepsilon)\hat{h} \tag{6.56}$$

with growth rate

$$\sigma(k,\varepsilon) = -\left(k^2 + \frac{5}{2}\right) + \frac{75}{112}MR + \varepsilon k^2\left(\frac{5}{448}MR - \frac{5}{4}\right) . \tag{6.57}$$

$\hat{h}(k,t)$ denotes the Fourier transform of $h(x,t)$ and

$$M = \frac{k^2}{k^4 + 24\,k^2 + 504} . \tag{6.58}$$

The simplicity of the formula for the growth rate enables us to write down the expression for the critical Rayleigh number as a function of the feedback control parameter,

$$R_c(\varepsilon) = \frac{28}{15}\frac{(4+5\varepsilon)\left(k_c^4 + 24k_c^2 + 504\right)^2}{(2\varepsilon - 5)\,k_c^4 + 84\varepsilon k_c^2 + 2520} . \tag{6.59}$$

where $k_c(\varepsilon)$ is the solution of the polynomial

$$(4+5\varepsilon)\left(\varepsilon k^8 + 120k^6\right) + \left(6360 + 4944\varepsilon - 2520\varepsilon^2\right)k^4 - 10080\varepsilon k^2 - 302400 = 0 . \tag{6.60}$$

For example when $\varepsilon = 0$ (uncontrolled Rayleigh-Bénard convection) we have $R_c = 1446$ and $k_c = 2.39$ compared to $R_c = 1296$ and $k_c = 2.55$ for the full problem, which a difference of about 12% and 6%, respectively. If we add just one more polynomial, we obtain $R_c = 1350$ and $k_c = 2.52$, which is just a difference of 4% and 1%, respectively. In figures 9 and 10 we compare both Galerkin approximations to the full model for a range a ε values. The model with two basis functions is included in the appendix.

In the following two figures we illustrate that our approximation indeed captures the nonlinear behavior of the full problem. In both figures we use the model with two basis function. In figure 11 we show the temperature and velocity fields for various ε. For the computations we used a finite difference scheme with a fully implicit Euler, on an x-domain of length $L = 40\pi/k_c(\varepsilon)$. where we use zero Dirichlet boundary conditions on both ends. When we compare

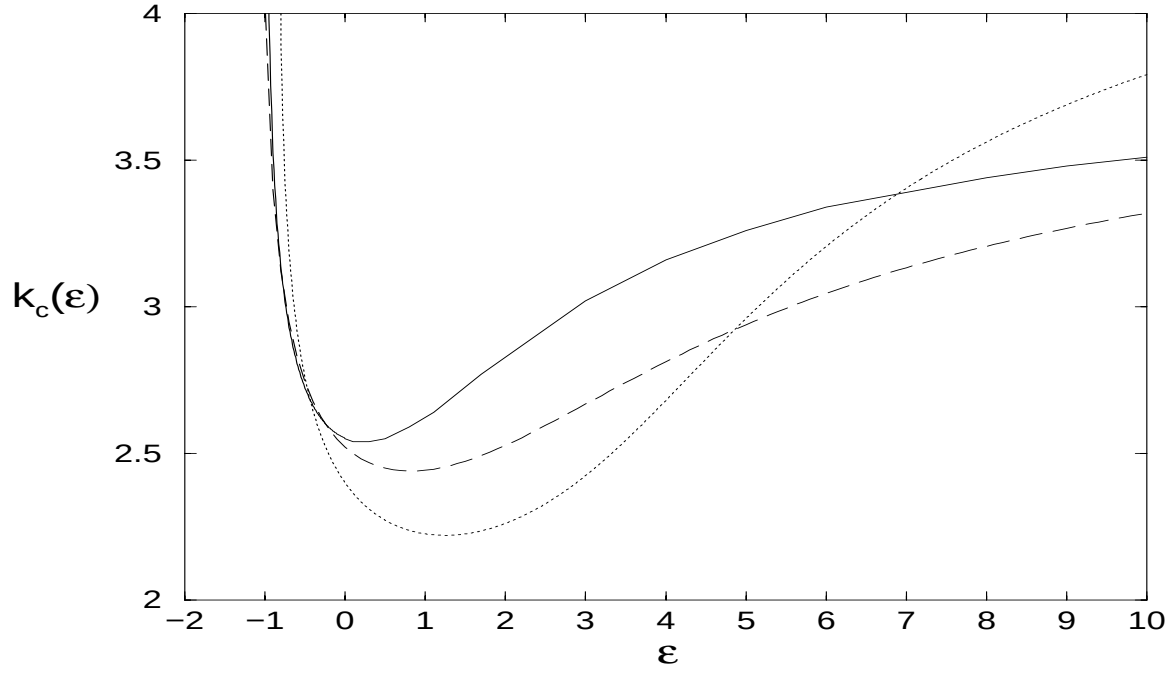

Figure 9: Comparison of the critical wavenumbers numbers $k_c(\varepsilon)$, resulting from the Galerkin approximation with one polynomial (dotted), two polynomials (dashed), and the full model (solid)

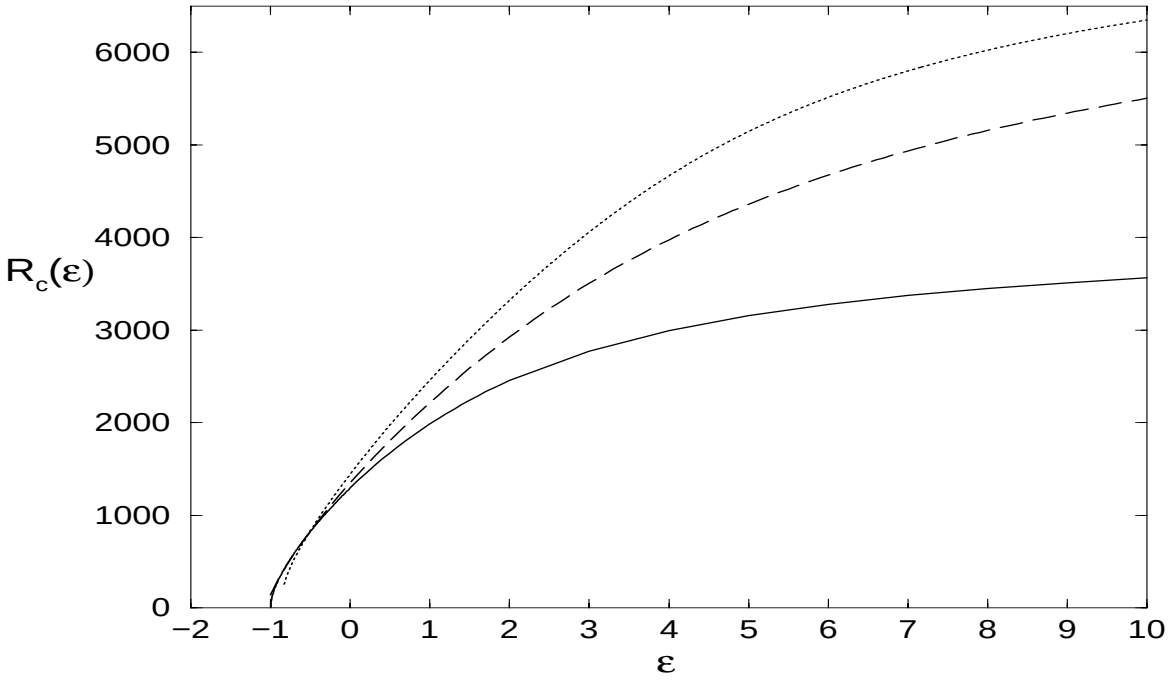

Figure 10: Comparison of the critical Rayleigh numbers $R_c(\varepsilon)$ resulting from the Galerkin approximation with one polynomial (dotted), two polynomials (dashed), and the full model (solid)

the portions in the middle, we note, that for $\varepsilon = -0.9$ the temperature has a more localized concentration, and the velocity field shows a higher number of rolls for $\varepsilon = -0.9$, while for $\varepsilon > 0$ the temperature field evens out and the number of rolls saturate.

When we take a look at the streamlines of the temperature field for the Galerkin model with periodic boundary conditions, for $\varepsilon = -0.9$ $\varepsilon = 0$, $\varepsilon = 0.9$ and compare them to the corresponding results of the 2D computation of the full problem, using a pseudo-spectral code with periodic boundary conditions, we observe very good agreements. We see that the Galerkin approximation captures the translations and distortions of the temperature field as ε is increased. We note that the patterns are a bit shifted in the vertical direction. The reason for this that the translation occurs slightly earlier for the full problem than for the Galerkin approximation. In all plots we let levels of the streamlines vary from -0.5 to 0.5 in increments of 0.02. The length of the x interval was scaled to $2\pi/k_c(\varepsilon)$.

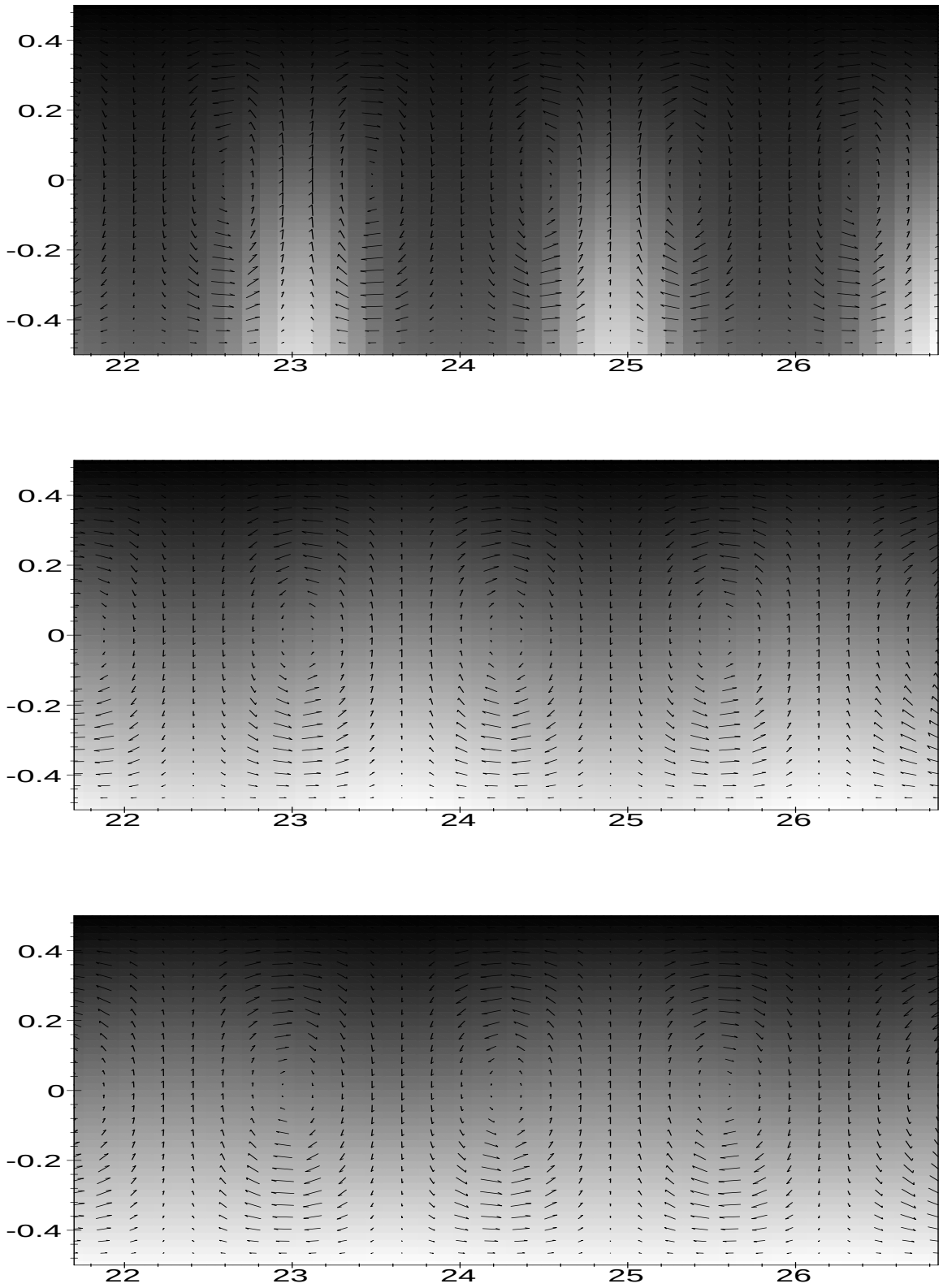

Figure 11: Temperature and Velocity fields for $\varepsilon = -0.9$ (top), $\varepsilon = 0$ (middle), $\varepsilon = 0.9$ (bottom)

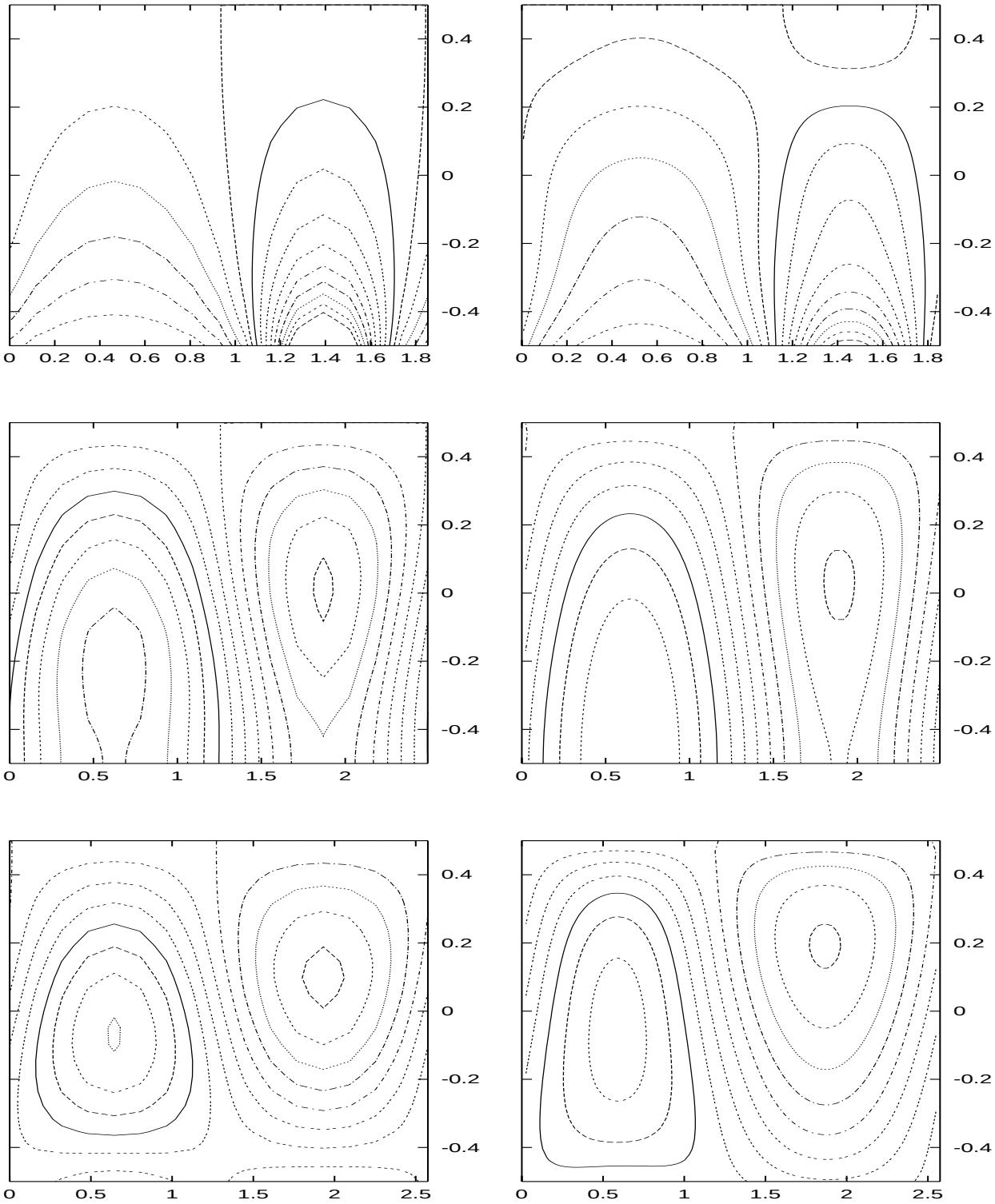

Figure 12: Streamlines for the temperature distributions for $\varepsilon = -0.9$ (top), $\varepsilon = 0$ (middle), $\varepsilon = 0.9$ (bottom). Figures on the left represent the nonlinear steady state of the full 2D problem, on the right are the corresponding distributions resulting from the Galerkin approximation with two polynomials.

6.2 Adding boundary effects

As can be seen from figure 9, the Galerkin approximations also capture the blow-up of the critical wavenumber for positive feedback control, while at the same time the critical Rayleigh number approaches zero. If we now also include boundary effects at the control boundary, the Fourier transformed problem (6.53)–(6.55) now has

$$\hat{s} = -\frac{2}{3}\gamma\hat{h} \tag{6.61}$$

with

$$\gamma = \frac{\frac{3}{2}k\sinh\left(\frac{k\delta}{2}\right) + \varepsilon k^2 e^{-k^2\lambda^2}}{1 + \frac{k}{8}\tanh\left(\frac{k\delta}{2}\right)\cosh\left(\frac{k\delta}{2}\right)} \tag{6.62}$$

instead of (6.55). The growth rate for the corresponding linear stability problem is

$$\sigma(k,\varepsilon) = -\left(k^2 + \frac{5}{2}\right) + \frac{75}{112}MR + \gamma\left(\frac{5}{448}MR - \frac{5}{4}\right) . \tag{6.63}$$

For our reduced model, the task of finding the most unstable wave numbers in the limit $\varepsilon \to -\infty$ reduces to determining the extrema of $\sigma(k,\varepsilon)$. In this limit, the dependence of the dominant wavenumber k_{mu} on δ, λ and R can implicitly be given by the formula

$$\begin{aligned} &k\tanh\left(\frac{k\delta}{2}\right)\left[\left(\frac{\lambda^2k^2}{2}+\delta\right)\left(\frac{R}{7M}-\frac{16}{M^2}\right)\frac{k^2}{4}+\frac{k^2}{M^2}+\left(k^4-24k^2-1512\right)\frac{R}{112}\right] \\ &+\left(\lambda^2+\frac{\delta}{32}\right)\left(\frac{R}{7M}-\frac{16}{M^2}\right)k^4+\frac{16k^2}{M^2}-\left(\frac{k^2}{42}+1\right)144R = 0 . \end{aligned} \tag{6.64}$$

Typically our positive feedback controlled problem with boundary effects is always unstable beyond a certain $\varepsilon^* < -1$, determined by the δ and λ. The most unstable wavenumber increases as δ and/or λ decrease. For fixed δ and λ the wavenumber asymptotes towards an upper bound as $\varepsilon \to -\infty$. The size of the band of unstable wavenumbers also asymptotes towards a value about twice the value of the most unstable wavenumber k_{mu}.

As an example we compare in the figure 13 the numerical results for the full model, again by using a pseudo-spectral method for (4.25)–(4.28) with (5.42) for the control boundary condition, to those of the Galerkin approximations, by using (6.63) and the corresponding formula for the problem with two polynomials. We let here $\delta = 0$ and $\lambda = 0.1$. We choose $R = 1000$ as well as $R = 0$, and note a relatively weak dependence on R for large negative ε. Thus for moderate R all curves can be seen to asymptote towards $k_{mu} = 1/\lambda$, a limit which can be easily obtained by inspection of equation (6.64) for $R \to 0$.

Thus, for containers typically used in those experiments, where e.g. $d = 0.794$cm with aspect ratios 1.6 and 8 for the x and y direction, we would expect for $\delta^* = \delta/d = 0.027$ and $\lambda* = \lambda/d = 0.4$ (i.e. 20 heaters) to observe rolls of size of about 1.26cm for large negative gain. The size of these rolls would typically increase as ε increases towards ε^*. Preliminary numerical computations, where boundary effects are implemented into our pseudo-spectral code, indicate that our model (3.6)-(3.8) does not determine a saturation temperature/velocity distribution. We expect that in practice, the maximal temperature and velocity is limited, for example, by the capacity of the heaters.

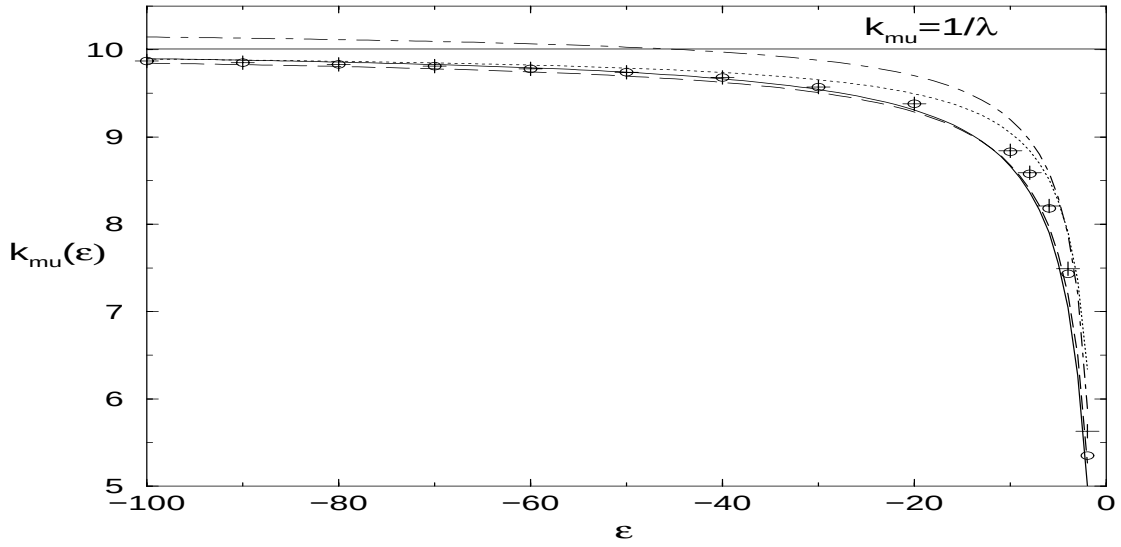

Figure 13: Most unstable wavenumbers $k_{mu}(\varepsilon)$ for $\delta = 0$ and $\lambda = 0.1$. Galerkin approximation with one polynomial for $R = 1000$ (dash-dot) and $R = 0$ (dotted), with two polynomials for $R = 1000$ (solid) and $R = 0$ (dashed), full problem for $R = 1000$ (circles) and $R = 0$ (crosses)

7 Discussion and further questions

In this paper we showed that Rayleigh-Bénard convection with positive feedback control via shadowgraphic measurement becomes ill-posed below a critical value $\varepsilon^\star$ of the control parameter, unless the details of the control boundaries such as heater size and boundary thickness are taken into account. For the resulting problem we developed a simpler model using a Galerkin approximation, which in effect reduced the dimension of our problem by one.

This model enabled us to reduce the task to determine the critical wavenumbers and Rayleigh numbers to solving polynomial equations, yielding good agreement with the full problem. Furthermore, we found, that by including boundary effects the problem will always be unstable below $\varepsilon^\star$ and the dominant wavenumbers in this regime are eventually determined by them. Furthermore, we could derive an asymptotic expression in the limit $\varepsilon \to -\infty$ for the dominant wavenumber as a function of the heater size, boundary thickness and Rayleigh number.

The good agreement of the Galerkin approximation and the full model even for a very small number of basis functions demonstrates the usefulness of such a method as a modeling tool. We can exploit this to investigate further aspects of controlled Rayleigh-Bénard convection. For example, we observe from figure 10 that R_c approaches a finite value as $\varepsilon \to \infty$. This means that the onset of the instability cannot be delayed to arbitrarily large Rayleigh numbers simply by increasing ε. This was already observed in [9]. The main reason for this limitation seems to be that we control the heat flux only at the lower boundary. Our Galerkin approximation (with one temperature polynomial H_0) shows that this control mechanism introduces a destabilizing term

$$\varepsilon k^2 \frac{5}{448} MR$$

(in equation 6.57) into the problem. A natural question that arises in this context is the question of the possibility to achieve perfect control. Ideally, such a control mechanism should equilibrate the heat flux at each point in the fluid layer. This can be achieved for our Galerkin approximation (one polynomial) by introducing heat sources into the bulk according to the distribution

$$s(x,t)H_0(z)\,.$$

In this case, the destabilizing term will be removed.

We also observed that applying this heat source distribution to the full model, as part of an alternative control mechanism, significantly increases the limiting R_c.

It would be interesting to know if for a Galerkin approximation with two polynomials a similar control mechanism could be constructed, resulting in a further increase of R_c. The question of existence of a perfect (bulk) control mechanism for the full problem would then reduce to the question of the convergence to a limiting heat source distribution as the number of polynomials goes to infinity.

Moreover, this method proves of even greater advantage when we investigate nonlinear stability. For example, in Wagner (2001) we derive amplitude equations for the velocity and the temperature from the governing Galerkin reduced equations. Because of the simplicity of the model this can be easily achieved by a formal asymptotic two-timing argument. Furthermore, we have extended our problem to the three-dimensional case, see Wagner (2001). The numerical simulations then reduce to a two-dimensional system of equations and prove to be useful for the study the effects of the lateral boundaries on the shape of the convection cells.

Acknowledgment

We would like to thank Andreas Münch for many stimulating discussions and A. Hosoi for introducing us to the Galerkin method. LEH would like to thank Michael Gustafson and Matt Brown for making the amplifier circuits used for these experiments. Acknowledgment is made to the Donors of The Petroleum Research Fund, administered by the American Chemical Society, for support of this work through grant ACS-PRF# 31645-G9. This work is supported by ONR grant N000140110290 and NSF grants DMS-9983320 and DMS-0074049.

Appendix

Galerkin approximation with two temperature functions

We let

$$T(x,z,t) = h(x,t)\,H_0(z) + f(x,t)\,H_1(z) + s(x,t)\,\ell_2(z)\,, \tag{7.65}$$

where $H_0(z)$ and $H_1(z)$ are chosen such that $H_0(1/2) = 0$ and $H_0'(-1/2) = 0$ as before, while the same conditions for $H_1(z)$ together with

$$\langle H_0, H_1 \rangle = 0 \tag{7.66}$$

yields a third order polynomial. We arrive at

$$H_0(z) = \left(z - \frac{1}{2}\right)\left(z + \frac{3}{2}\right), \tag{7.67}$$

$$H_1(z) = \left(z - \frac{1}{2}\right)\left(z^2 + \frac{29}{32}z + \frac{7}{64}\right). \tag{7.68}$$

The polynomial $\ell_2(z)$ naturally must satify $\ell_2(1/2) = 0$. The order will be further increased by requiring the boundary condition at $z = -1/2$ to be satisfied. However, in order to avoid artificial singularities, not present in the full problem, requires

$$\rho_2 = \int_{-1/2}^{1/2} \ell_2(z)\, dz = \langle \ell_2, H_0 \rangle \int_{-1/2}^{1/2} H_0(z)\, dz + \langle \ell_2, H_1 \rangle \int_{-1/2}^{1/2} H_1(z)\, dz \tag{7.69}$$

to be satisfied. Calculations can be further simplified, if we choose $\ell_2(z)$ to also be orthogonal to H_0 and H_1. As a consequence, we obtain a polynomial of fourth order such that $\rho_2 = 0$ and normalize it such that $\ell_2'(-1/2) = 1$. This yields

$$\ell_2(z) = -\frac{7}{4}\left(z - \frac{1}{2}\right)\left(z^3 + \frac{1}{10}z^2 - \frac{17}{140}z - \frac{1}{280}\right). \tag{7.70}$$

We can now derive the new model equations by testing the full problem with the test functions

$$\theta_0 = \delta(x)\,\mu_z(z), \qquad \theta_1 = -\delta'(x)\,\mu_z(z), \tag{7.71}$$

$$\phi_0 = \delta(x) H_0(z), \qquad \phi_1 = \delta(x) H_1(z), \tag{7.72}$$

to obtain

$$u_{xxxx} - 24\,u_{xx} + 504\,u = -R\left(60\,h + \frac{27}{8}\,f - \frac{1}{5}\,s\right)_x , \tag{7.73}$$

$$\begin{aligned} h_t - h_{xx} + \frac{5}{2}\,h + \frac{9}{448}\left(h_x u + \frac{1}{2}\,h u_x\right) &= -\frac{5}{64}\,f + \frac{15}{8}\,s + \frac{5}{448}\,u_x \\ &\quad + \frac{1}{448}\left(\frac{97}{96} f_x u + \frac{91}{64}\,f u_x\right) \\ &\quad + \frac{1}{448\cdot 20}\left(3\,s_x u + \frac{37}{12}\,s u_x\right) , \end{aligned} \tag{7.74}$$

$$\begin{aligned} f_t - f_{xx} + \frac{3059}{130}\,f - \frac{173}{390\cdot 32}\left(f_x u + \frac{1}{2}\,f u_x\right) &= -\frac{112}{13}\,h - \frac{6132}{325}\,s + \frac{9}{130}\,u_x \\ &\quad + \frac{1}{390}\left(97\,h_x u - \frac{79}{2}\,h u_x\right) \\ &\quad + \frac{1}{429\cdot 200}\left(31\,s_x u + \frac{3\cdot 329}{4}\,s u_x\right) , \end{aligned} \tag{7.75}$$

$$\text{with} \quad s = \varepsilon\left(\frac{2}{3}\,h_{xx} + \frac{1}{48}\,f_{xx}\right) . \tag{7.76}$$

Linear stability

We linearize about the conductive state to get

$$u_{xxxx} - 24\,u_{xx} + 504\,u = -R\left(60\,h + \frac{27}{8}\,f - \frac{1}{5}\,s\right)_x , \tag{7.77}$$

$$h_t - h_{xx} + \frac{5}{2}\,h = -\frac{5}{64}\,f + \frac{15}{8}\,s + \frac{5}{448}\,u_x , \tag{7.78}$$

$$f_t - f_{xx} + \frac{3059}{130}\,f = -\frac{112}{13}\,h - \frac{6132}{325}\,s + \frac{9}{130}\,u_x , \tag{7.79}$$

$$\text{with} \quad s = \varepsilon\left(\frac{2}{3}\,h_{xx} + \frac{1}{48}\,f_{xx}\right) . \tag{7.80}$$

The Fourier transform of above equations yields

$$\hat{h}_t = -\left(k^2 + \frac{5}{2}\right)\,\hat{h} - \frac{5}{64}\,\hat{f} + \frac{15}{8}\,\hat{s} + \frac{5}{448}\,i\,k\,\hat{u}\,, \tag{7.81}$$

$$\hat{f}_t = -\left(k^2 + \frac{3059}{130}\right)\,\hat{f} - \frac{112}{13}\,\hat{h} - \frac{6132}{325}\,\hat{s} + \frac{9}{130}\,i\,k\,\hat{u}\,, \tag{7.82}$$

$$\text{where} \quad \hat{s} = -\varepsilon\,k^2\left(\frac{2}{3}\,\hat{h} + \frac{1}{48}\,\hat{f}\right) \quad \text{and} \quad i\,k\,\hat{u} = M\,R\left(60\,\hat{h} + \frac{27}{8}\,\hat{f} - \frac{1}{5}\,\hat{s}\right)\,. \tag{7.83}$$

The solution of (7.81)–(7.82) is

$$\hat{h}(k,t) = K_1\,a_1\,\exp(\sigma_1\,t) + K_2\,a_2\,\exp(\sigma_2\,t)\,, \tag{7.84}$$

$$\hat{f}(k,t) = K_1\,\exp(\sigma_1\,t) + K_2\,\exp(\sigma_2\,t)\,, \tag{7.85}$$

where K_1 and K_2 are constants and

$$a_1 = \frac{1}{2D}\left(A - C + \sqrt{(A-C)^2 + 4DB}\right)\,,\; a_2 = \frac{1}{2D}\left(A - C - \sqrt{(A-C)^2 + 4DB}\right)\,, \tag{7.86}$$

$$\sigma_1 = \frac{1}{2}\left(A + C + \sqrt{(A-C)^2 + 4DB}\right)\,, \quad \sigma_2 = \frac{1}{2}\left(A + C - \sqrt{(A-C)^2 + 4DB}\right)\,, \tag{7.87}$$

with

$$A(k^2,\varepsilon) = -k^2 - \frac{5}{2} + \mathrm{R}\frac{5}{448}\left(60 + \frac{2}{15}\varepsilon k^2\right)M - \frac{5}{4}\varepsilon k^2\,, \tag{7.88}$$

$$B(k^2,\varepsilon) = \mathrm{R}\frac{5}{448}\left(\frac{27}{8} + \frac{1}{240}\varepsilon k^2\right)M - \frac{5}{64} - \frac{5}{128}\varepsilon k^2\,, \tag{7.89}$$

$$C(k^2,\varepsilon) = -k^2 - \frac{3059}{130} + \mathrm{R}\frac{9}{130}\left(\frac{27}{8} + \frac{1}{240}\varepsilon k^2\right)M + \frac{511}{1300}\varepsilon k^2\,, \tag{7.90}$$

$$D(k^2,\varepsilon) = \mathrm{R}\frac{9}{130}\left(60 + \frac{2}{15}\varepsilon k^2\right)M - \frac{112}{13} + \frac{4088}{325}\varepsilon k^2\,. \tag{7.91}$$

From this we calculate the critical Rayleigh numbers $R_c(\varepsilon)$ and critical wavenumbers $k_c(\varepsilon)$, by solving for the dominant growth rate σ_1

$$\sigma_1 = 0 \quad \text{and} \quad \frac{\partial\sigma_1}{\partial R} = 0\,. \tag{7.92}$$

References

[1] BÉNARD, H. 1900. Les tourbillons cellulaires dans une nappe liquide. *Rev. Gén. Sciences Pure Appl.* **11**, 1261–1271.

[2] BÉNARD, H. 1901. Les tourbillons cellulaires dans une nappe liquide transportant de la chaleur par convection en régime permanent. *Ann. Chim. Phys.* **23**, 62–144.

[3] BUSSE, F. H. 1962. *Das Stabilitätsverhalten der Zellkonvektion bei endlicher Amplitude.* Dissertation, (Univ. München).

[4] BUSSE, F. H. 1967. The stability of finite amplitude cellular convection and its relation to an extremum principal. *J. Fluid Mech.* **30**, 625–649.

[5] CROSS, M. C. & HOHENBERG, P.C. 1993. Pattern formation outside of equilibrium. *Rev. Mod. Physics* **65**, 851–1112.

[6] DUPONT, T. F. AND HOSOI, A. E. 1999 A reduced-dimension model for Rayleigh-Bénard convection *preprint.*

[7] GETLING, A. V. 1998. *Rayleigh-Bénard Convection Structures and Dynamics.* Word Scientific. Singapore.

[8] GUSTAFSON, M.R. & HOWLE. L.E. 1999. Effects of anisotropy and boundary plates on the critical values of a porous medium heated from below.*Int. J. Heat Mass Trans.* **42**, 3419-3420.

[9] HOWLE, L. E. 1997a. Control of Rayleigh-Bénard convection in a small aspect ratio container. *Int. J. Heat Mass Trans.* **40**, 817–822.

[10] HOWLE, L. E. 1997b. Active control of Rayleigh-Bénard convection. *Phys. Fluids* **9**, 1861–1863.

[11] HOWLE, L. E. 1997c. Linear stability analysis of controlled Rayleigh-Bénard convection using shadowgraphic measurement. *Phys. Fluids* **9**, 3111–3113.

[12] HOWLE, L. E. 2000. The effect of boundary properties on controlled Rayleigh-Bénard convection. *J. Fluid Mech.* **411**, 39–58.

[13] HOWLE, L. E. 2001. Proportional and differential convection of Rayleigh-Bénard convection. *J. Fluid Mech.* to be submitted.

[14] MANNEVILLE, P. 1990. *Dissipative Structures and Weak Turbulence*, Academic Press, Inc., New York.

[15] MÜLLER, G. 1988. *Crystals: Growth, Properties, and Applications; 12: Convection and Inhomogeneities in Crystal Growth from the Melt.* H.C. Freyhardt *et al.*, eds. Springer-Verlag.

[16] ORSZAG, S.A., THESS, A. 1995. Surface-tension-driven Bénard convection at infinite Prandtl number. *J.Fluid Mech.* **283**, 201–229.

[17] Or, A.C., Cortelezzi, L, Speyer, J.L. 2001. Robust feedback control of Rayleigh-Bénard convection. *J.Fluid Mech.* **437**, 175–202.

[18] Lord Rayleigh 1916. On convection currents in a horizontal layer of fluid, when the higher temperature is on the under side. *Phil. Mag.* **32**, 529–546.

[19] Tang, J. & Bau, H. H. 1993a. Stabilization of the no-motion state in Rayleigh-Bénard convection through the use of feedback control. *Phys. Rev. Lett.* **70**, 1795–1798.

[20] Tang, J. & Bau, H.H. 1993b. Feedback control stabilization of the no-motion state of a fluid confined in a horizontal, porous layer heated from below. *J. Fluid Mech.***257**, 485–505.

[21] Tang, J. & Bau, H.H. 1995. Stabilization of the no-motion state of a horizontal fluid layer heated from below with Joule heating. *Trans. ASME: J. Heat Trans.***117**, 329–333.

[22] Wagner, B. A. 2001. Nonlinear aspects of controlled Rayleigh-Bénard convection, to be submitted